ACS OMEGA

Open Access

http://pubs.acs.org/journal/acsodf

Article

Functionalized Metal-Free Carbon Nanosphere Catalyst for the Selective C−N Bond Formation under Open-Air Conditions

Kumar Krishan, Bhattu Swapna, Ankit Kumar Chourasia, Chandra S. Sharma, and Putla Sudarsanam*

Cite This: *ACS Omega* 2024, 9, 35676−35685

Read Online

ACCESS | Metrics & More | Article Recommendations | Supporting Information

ABSTRACT: A versatile shape-controlled carbon nanomaterial that can efficiently catalyze the selective C−N coupling reactions under metal-free and open-air conditions was developed by applying N-doping and KOH activation strategies in candle soot (ANCS). The TEM and elemental mapping results showed the formation of sphere-shaped carbon particles as well as the uniform distribution of nitrogen species in the carbon framework. KOH activation enhanced the specific surface area of carbon, whereas N-doping enriched the electron-deficient nature by introducing functional N-based pyrrolic/graphitic structures in the carbon framework. The synergistic effect of N-doping and KOH activation significantly improved the catalytic efficiency of the carbon catalyst (ANCS), giving a 96% conversion of *o*-phenylenediamine (OPD) with a good selectivity to 2-phenylbenzimidazole (97%). In contrast, the pristine carbon exhibited very low activity (48% conversion of the OPD and 36% selectivity to 2-phenylbenzimidazole). Besides, the ANCS nanomaterial provided a facile catalytic approach for the homo- and cross-C−N condensation of various aromatic amines and diamines to produce diverse functional imines and benzimidazoles at mild conditions. This work provided promising insights into developing advanced, metal-free carbon-based catalysts for selective C−N coupling reactions to produce valuable drug motifs.

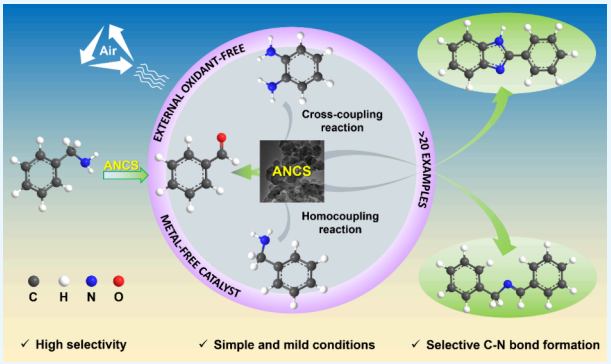

1. INTRODUCTION

Transition metals are the essential components of numerous industrially used heterogeneous catalysts.[1] However, their expensive nature and rapid catalytic deactivation impose several practical limitations. Thus, developing efficient metal-free catalysts is a primary goal of the catalysis community. Carbon-based materials have received significant attention for heterogeneous catalysis because of the unique properties of carbon, such as high abundance, low cost, remarkable hydrothermal stability, tunable porosity, and high specific surface area.[2,3] Another vital advantage of carbon materials is their facile functionalization either by acid or base molecules or by elements based on the target catalytic application, while tuning their porous framework to achieve enhanced diffusion properties. Thus, the fine engineering of the structure and porosity of carbon could provide potential strategies for developing multifunctional carbon-based materials with selective catalytic properties for the chemical industry.

The carbon−nitrogen (C−N) coupling is a pivotal chemical reaction for producing diverse nitrogenous organic compounds for the pharma industry.[4−12] In particular, benzimidazole-based compounds are widely used drugs for various medical treatments (Figure 1). The coupling of benzylamine with *o*-phenylenediamine (OPD) gives 2-phenylbenzimidazole.[8] However, this reaction typically requires a strong oxidant (TBHP, H_2O_2, or molecular oxygen) to accelerate the oxidative dehydrogenation of benzylamine to the benzaldehyde intermediate, which then reacts with OPD to give 2-phenylbenzimidazole. A similar mechanism can also be expected in the other C−N condensation of aromatic amines. Using air as the oxidant for the selective C−N condensation with an efficient metal-free heterogeneous catalyst has great promise in terms of both economic and eco-friendly points of view.[12−14]

Several types of carbon materials, such as carbon black, mesoporous carbon, graphene, carbon nanofibers, and carbon nanotubes, have been developed for various applications, including heterogeneous catalysis.[15,16] In recent years, candle soot (CS) nanospheres have emerged as versatile carbon nanomaterials because of their well-controlled particle size/morphology, high specific surface area, tunable porosity, and efficient functionalization.[17,18] The CS nanospheres can be efficiently synthesized by using a facile combustion approach of the candles. The morphology of carbon nanospheres allows for efficient functionalization, expanding their applications in

Received: April 25, 2024
Revised: July 25, 2024
Accepted: July 30, 2024
Published: August 8, 2024

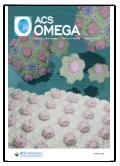

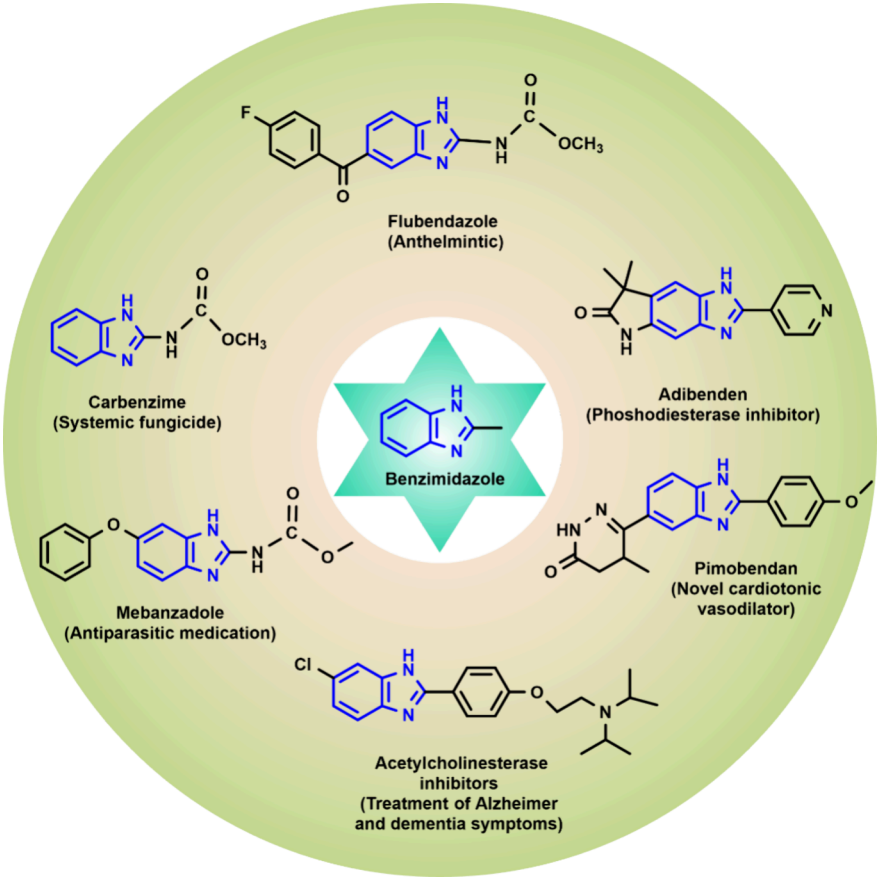

Figure 1. Benzimidazole-based drug molecules.

heterogeneous catalysis, adsorption, gas separation, energy storage, and drug delivery.[19] The waving flake curvature structure of the carbon nanospheres provides more active edge sites and dangling bonds for heterogeneous catalytic applications.[20] Another advantage of carbon nanospheres is their interconnected graphitic network, which can control the mass diffusion properties of the reactants, intermediates, and products to achieve higher yields of the desired products at mild reaction conditions. The CS nanospheres can exhibit good dispersion in various organic solvents and reagents because of their flexible carbon structure, enabling them to be promising catalytic materials for various organic chemical reactions.

KOH activation and N-doping are two fundamental strategies widely investigated to develop functional carbon materials. These strategies can tune the porous framework of carbon while introducing functional groups and defect sites in its structure. On the one hand, the redox reactions of carbon with KOH facilitate the intercalation of metallic K between the carbon lattices.[21] The subsequent removal of K results in increased porosity and a higher specific surface area. The KOH concentration and the activation temperature determine the reactions between carbon and KOH, and the consequent porous structure and surface area. On the other hand, replacing some carbon atoms with N dopants in the carbon framework creates electron-deficient carbon as the inserted N pulls the electron density from the adjacent carbon because of its higher electronegativity than the carbon.[22−25] The electron-deficient carbon, acting as the Lewis acid site, can interact with nucleophilic molecules like benzylamine to accelerate the C−N coupling reactions.[2,26] The inserted N species can also act as Lewis basic sites. Thus, N-doped carbon materials can be used for both acid- and base-catalyzed reactions. Moreover, N-doping can introduce various N-heterocycles, such as pyridinic-N, pyrrolic-N, graphitic-N (or quaternary-N), and pyridinic-N-oxide, depending on the reagents used, preparation method, and postsynthesis activation strategy. The unique features of bonding and coordination configurations of N-doped heterocyclic structures can selectively influence the activity of carbon catalysts for specific catalytic applications. The nucleophilic nature of the nitrogen of these species can enhance the interaction of the carbon catalyst with the electron-deficient intermediates (e.g., benzaldehyde) for achieving higher reaction rates in the C−N condensation reactions.[27] These promising benefits motivated us to develop a functional CS nanomaterial. In this work, we used a simple combustion process to prepare well-defined CS nanospheres with homogeneous particle sizes and morphology. The CS nanospheres are effectively functionalized by treatment with melamine (nitrogen source) and then KOH activation. Another advantage of carbon nanospheres is their interconnected graphitic network, which can control mass diffusion properties of the reactants, intermediates, and products to achieve higher yields of the desired products at mild reaction conditions. The developed carbon materials were characterized by using various analytical techniques to elucidate their properties in comparison to those of the pristine CS material. The ANCS catalyst was found to be highly active for the C−N condensation reactions to synthesize diverse imines and benzimidazoles without using any external oxidizing reagent, highlighting the eco-friendly and economic aspects of this work for organic chemistry.

https://doi.org/10.1021/acsomega.4c03987
ACS Omega 2024, 9, 35676−35685

2. EXPERIMENTAL SECTION

A detailed procedure of the synthesis, characterization, and catalytic activity of the carbon materials is provided in the Supporting Information.

3. RESULTS AND DISCUSSION

3.1. Characterization Studies. The TEM analysis is carried out to elucidate the morphology and particle size of the carbon materials (Figure 2). The CS sample contains well-

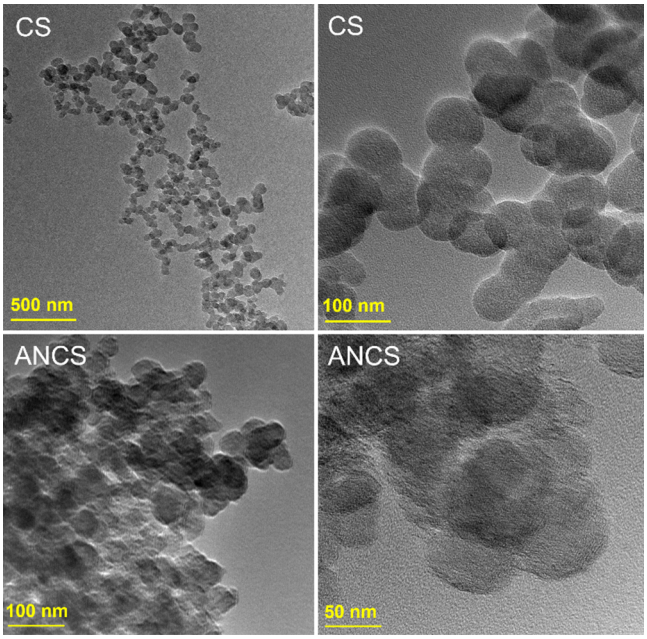

Figure 2. TEM images of the CS and ANCS materials.

defined spherical particles (particle size is 70−85 nm), which are interlinked to form aggregates with large voids.[28] The ANCS sample also contains spherical-shaped carbon particles with a particle size of 50−75 nm. The STEM-EDX analysis confirmed the uniform dispersion of carbon, oxygen, and nitrogen species in the ANCS catalyst (Figure 3). Especially, the uniform incorporation of nitrogen can provide N-based functional groups in the carbon framework, which could play a crucial role in the C−N coupling reactions. All the carbon materials showed type IV isotherms (Figure S1, Supporting Information). The CS and ANCS materials showed a typical H3-type hysteresis loop, which represents slit-shaped voids in the aggregates of carbon spheres. In contrast, the ACS material showed an H4-type hysteresis loop corresponding to narrow slit-shaped voids. The presence of voids (Figure 2) formed by interlinked aggregates of spherical particles could be the reason for the observed hysteresis loops. The BET surface area of the CS nanomaterial was found to be 276 m^2/g (Table S1, Supporting Information). The activation of the CS nanomaterial with KOH significantly increased the BET surface area (2050 m^2/g for ACS). However, the N-doping, followed by KOH activation, led to a decrease in BET surface area (1596 m^2/g for ANCS), which could be due to the aggregation of the particles and/or structural changes in the carbon framework. The mean pore volume and pore diameter of the carbon materials were found to be in the range of 0.8−1.8 cc/g and 2.8−12 nm, respectively (Table S1, Supporting Information).

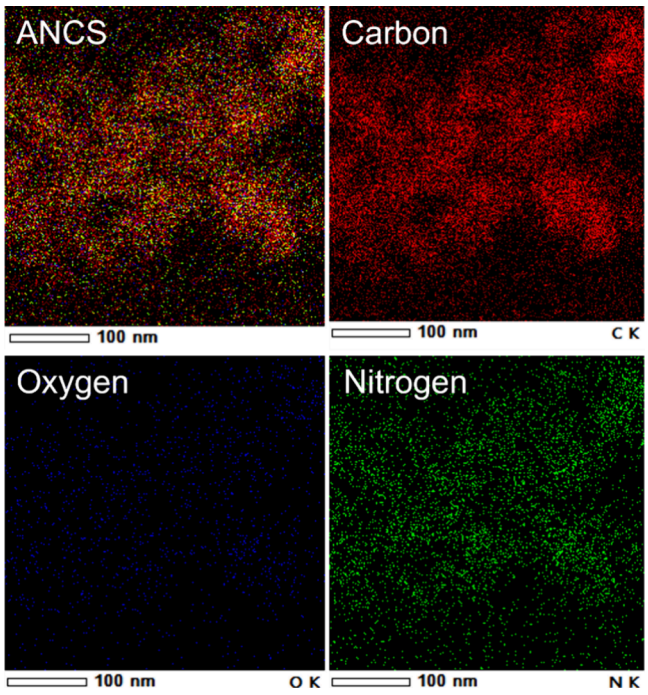

Figure 3. STEM-EDAX elemental mapping images of the ANCS catalyst.

The powder XRD data showed a broad diffraction peak at 2 theta of 25.2° in the CS sample, which belongs to the (002) plane of the graphene sheets (Figure 4a).[29,30] The broadness of the graphitic (002) plane was increased in ACS and ANCS samples, which is due to the increased defects along with variation in the interlayer stacking of the graphene sheets due to the KOH activation and N-doping. The ACS and ANCS samples show an additional broad XRD peak at 2 theta of 43.7°, corresponding to the (100) plane of the graphitic structure. The Raman spectra of all the samples showed two bands at 1349 and 1589 cm^{-1}, which belong to the defective (D) and graphitic (G) nature of the carbon, respectively (Figure 4b).[31,32] The defective D band can denote disordered carbon, structural defects, and/or the defunctionalization of oxygen-based species in carbon materials. The I_D/I_G ratio represents the relative number of defect sites in the carbon framework. The ANCS sample contains a higher ratio of I_D/I_G (1.53) in comparison to the ACS (1.26) and CS (0.86) samples. This is due to the replacement of carbon atoms in the graphitic structure with nitrogen atoms, forming nitrogen-based functional groups with disordered carbon and structural defects in the ANCS sample, which was elucidated by FT-IR, EPR, and XPS analyses in the following sections.

The FT-IR analysis was conducted to identify the functional groups in the carbon materials (Figure 5a). All the samples exhibit a broad peak in the range 3300−3500 cm^{-1} belonging to functional hydroxyl (−OH) and/or amine (−NH) groups. The pure CS sample shows several peaks belonging to −C−O (1238 cm^{-1}), −C=C (1596 cm^{-1}), −COOH/−C=O (1730 cm^{-1}), and −OH (3418 cm^{-1}) groups.[26,33] These peaks are not found in the ACS sample, which is due to the removal of oxygen-containing groups by KOH activation. In the place of oxygen functional groups, various N-based functional groups (−C−N; 1144 cm^{-1}, −C=N; 1587 cm^{-1}, and −NH; 3449 cm^{-1}) were noticed in the ANCS sample, indicating the N-doping in the carbon structure, in line with the Raman studies (Figure 4b). An

https://doi.org/10.1021/acsomega.4c03987
ACS Omega 2024, 9, 35676−35685

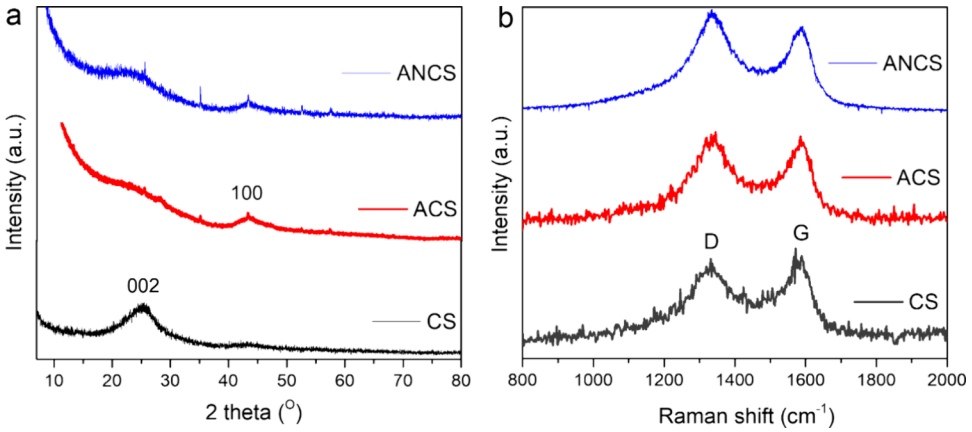

Figure 4. (a) Powder XRD patterns and (b) Raman spectra of candle soot (CS), activated candle soot (ACS), and activated N-doped candle soot (ANCS) catalysts.

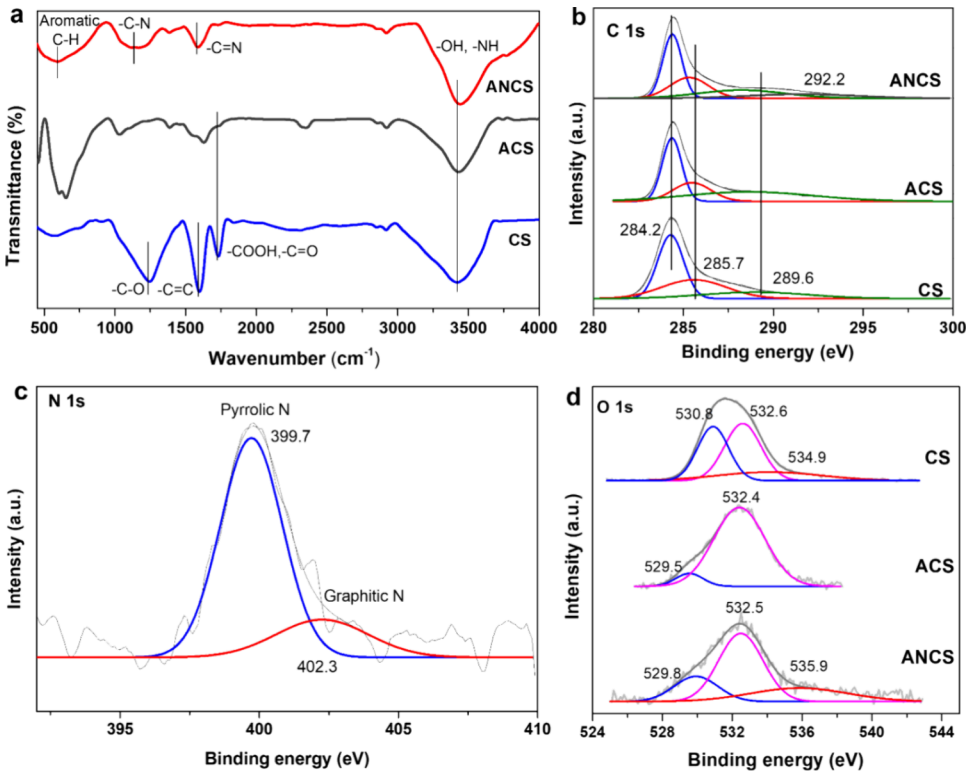

Figure 5. (a) FT-IR spectra and (b) C 1s XPS, (c) N 1s XPS, and (d) O 1s XPS of candle soot (CS), activated candle soot (ACS), and activated N-doped candle soot (ANCS) catalysts.

FT-IR peak corresponding to the aromatic methyl group (−CH; 593 cm^{-1}) is observed only in the case of the ANCS sample.[26,33] The EPR analysis showed that the ACS and ANCS catalysts exhibit broader EPR signals and lower *g*-values as compared to the pure CS catalyst (Figure S2, Supporting Information). This indicates the perturbations in the electronic and surface structure of the carbon framework after the KOH and N-doping treatments.[34,35] A decrease in the *g*-value of the ACS and ANCS catalysts compared to the pure CS catalyst indicates a decrease in the degree of oxidation of the carbon in ACS and ANCS catalysts. The increased width of the EPR peaks reveals an increased BET surface area of ACS and ANCS catalysts compared to the CS catalyst (Table S1, Supporting Information).[35] Though the EPR analysis is used to estimate the defect density in the carbon materials, it must be indicated that the EPR technique cannot detect all defects present in the carbon framework.[34]

The XPS analysis was conducted to elucidate the nature of carbon, nitrogen, and oxygen species in the carbon catalysts. The C 1s XP spectrum of pure CS shows three major peaks at the binding energies (BEs) of 284.2, 285.7, and 289.6 eV, corresponding to the carbon species of C=C, C−O, and O−C=O groups, respectively (Figure 5b).[30] The close observation of Figure 5b reveals that the major C 1s peak (284.2 eV) belonging to C=C in the CS sample is shifted to higher BEs in the ACS and ANCS samples, whereas the C 1s peaks of the C−O and O−C=O groups are shifted to lower BEs. The ANCS sample exhibits an additional peak at 292.2 eV, corresponding to carbon species in the N−C=O group, confirming the N-doping in the carbon structure. The N 1s XP spectrum of the ANCS

https://doi.org/10.1021/acsomega.4c03987
ACS Omega 2024, 9, 35676−35685

sample shows two peaks at 399.7 and 402.3 eV, which belong to pyrrolic and graphitic nitrogen, respectively (Figure 5c).[26,36] The pyrrolic nitrogen is dominant in the ANCS sample. The CS sample shows three O 1s XPS peaks at 530.8, 532.6, and 534.9 eV, corresponding to oxygen in the C=O, C−O, and O=C−OH groups, respectively (Figure 5d).[26] The ACS sample does not contain the third O 1s peak (O=C−OH group), indicating the selective defunctionalization of acidic groups in carbon by KOH (base). The exposure of the KOH/CS mixture to the temperature of 900 °C promotes the reaction of the KOH base with the oxygen-containing acidic functional groups of CS, resulting in the removal of O=C−OH groups from the carbon matrix.[37,38] Applying higher temperatures (900 °C) after the KOH treatment can also remove the oxygen-containing groups from the carbon matrix in the form of oxygen, carbon dioxide, and water.[39] However, the ANCS sample exhibited the third O 1s peak, corresponding to the O=C−OH group (Figure 5d). This indicates that KOH activation is not very effective for N-doped CS material to defunctionalize oxygen species. The reason is that the inserted N species in the carbon matrix can exhibit a strong electrostatic interaction with the O=C−OH groups, which are very difficult to defunctionalize by the KOH treatment.[40,41] The elemental compositions of carbon, nitrogen, oxygen, and hydrogen in the ANCS catalyst, estimated by CHNO analysis, were found to be 95.78, 1.31, 2.46, and 0.45 wt %, respectively. However, a very low N amount (0.39 wt %) was found by the XPS analysis as it is a surface-sensitive technique and cannot detect the total nitrogen amount in the ANCS catalyst.

The catalyst's acid sites (Brønsted and Lewis), especially Lewis acid sites, play a crucial role in the C−N coupling reactions.[11,12] The electron-deficient carbon in the developed carbon catalysts can act as the Lewis acid sites (LA), and the hydroxyl and carboxyl species are the Brønsted acid sites (BA). The pyridine-adsorbed FT-IR analysis of carbon catalysts is conducted to estimate the nature of the acid sites (Figure 6).

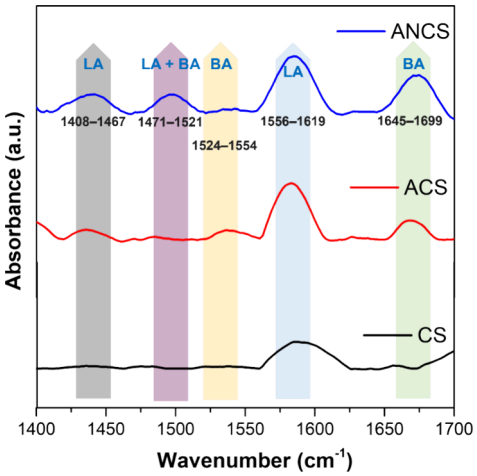

Figure 6. Pyridine-adsorbed FT-IR spectra of the CS, ACS, and ANCS catalysts.

The noticed FT-IR peaks in the range of 1408−1467, 1471−1521, 1524−1554, 1556−1619, and 1645−1699 cm^{-1} are assigned to LA, LA + BA, BA, LA, and BA, respectively (Figure 6).[11,42] The CS sample contains only one peak at 1556−1619 cm^{-1}, corresponding to LA sites. In contrast, the ACS and ANCS samples contain both BA and LA sites' peaks, but their intensity is lower in the ACS sample compared to the ANCS sample. It indicates the presence of more Lewis and Brønsted acid sites in the ANCS catalyst.

4. CATALYTIC ACTIVITY STUDIES

4.1. C−N Coupling of OPD with Benzylamine Using Carbon Nanomaterials. The catalytic efficiency of the developed carbon materials was investigated for the synthesis of 2-phenylbenzimidazole via cascade C−N coupling of OPD with benzylamine using a 1.5:2.5 molar ratio of OPD and benzylamine in toluene solvent at a 4 h reaction time and 100 °C reaction temperature under open-air conditions. In the blank case (i.e., without the catalyst), no noticeable conversion of OPD was found (entry 1, Table 1). The observed OPD conversion and product selectivity over the developed carbon nanomaterials (entries 2−4, Table 1) at the same reaction conditions employed for the blank test indicate their catalytic efficacy in the C−N condensation reaction under metal-free and open-air conditions. Pure CS material gave 48% conversion of the OPD, but very low selectivity to 2-phenylbenzimidazole (36%) was achieved (entry 2, Table 1). In the case of the ACS catalyst, both the level of conversion of OPD (76%) and 2-phenylbenzimidazole (82%) was significantly increased (entry 3, Table 1). The best results were found with the ANCS catalyst, which gave 89% conversion with 90% 2-phenylbenzimidazole selectivity (entry 4, Table 1). With the increase of reaction time from 4 to 5 h, the ANCS catalyst gave 96% conversion of OPD and 97% 2-phenylbenzimidazole selectivity (entry 5, Table 2). With 5 and 10 wt % of the ANCS catalyst, low conversion/selectivity was obtained (entries 6 and 7, Table 1), respectively. Under the inert atmospheric conditions (i.e., N_2), the level of the OPD conversion was very low (entry 8, Table 1), indicating the necessity of air for the C−N coupling reaction.

Table 1. C−N Coupling of Benzylamine and OPD Using Various Carbon-Based Catalysts[a]

s. no.	catalyst	OPD conversion (%)	benzimidazole selectivity (%)	other products
1	blank	negligible		
2	CS	48	36	64
3	ACS	76	82	18
4	ANCS	89	90	10
5[b]	ANCS	96	97	3
6[c]	ANCS	58	39	61
7[d]	ANCS	82	81	19
8[e]	ANCS	8	61	39

[a]1.5 mmol *o*-phenylenediamine (OPD), 2.5 mmol benzylamine, 15 wt % catalyst with respect to OPD, 100 °C, 4 h, toluene (1 mL), and open-air conditions. [b]5 h. [c]5 wt % catalyst. [d]10 wt % catalyst. [e]Inert atmospheric condition (N_2 gas).

4.2. Kinetic and Hot-Filtration Studies in the C−N Coupling of Benzylamine and OPD Using the ANCS Catalyst. The effect of reaction temperature from 1 to 5 h in the coupling of benzylamine and OPD using the ANCS catalyst was conducted at 100 °C in toluene solvent (Figure 7a). Both the conversion of OPD and product selectivity were rapidly increased with the increase of reaction time up to 3 h. This is due to the availability of high concentrations of reactants until 3 h, accelerating the forward reaction toward benzimidazole formation. After 3 h of reaction time, the reaction faces equilibrium limitations, resulting in a trivial increase in OPD

https://doi.org/10.1021/acsomega.4c03987
ACS Omega 2024, 9, 35676−35685

Table 2. Substrate Scope in the C−N Coupling of Benzylamine and OPD Using the ANCS Catalyst[a]

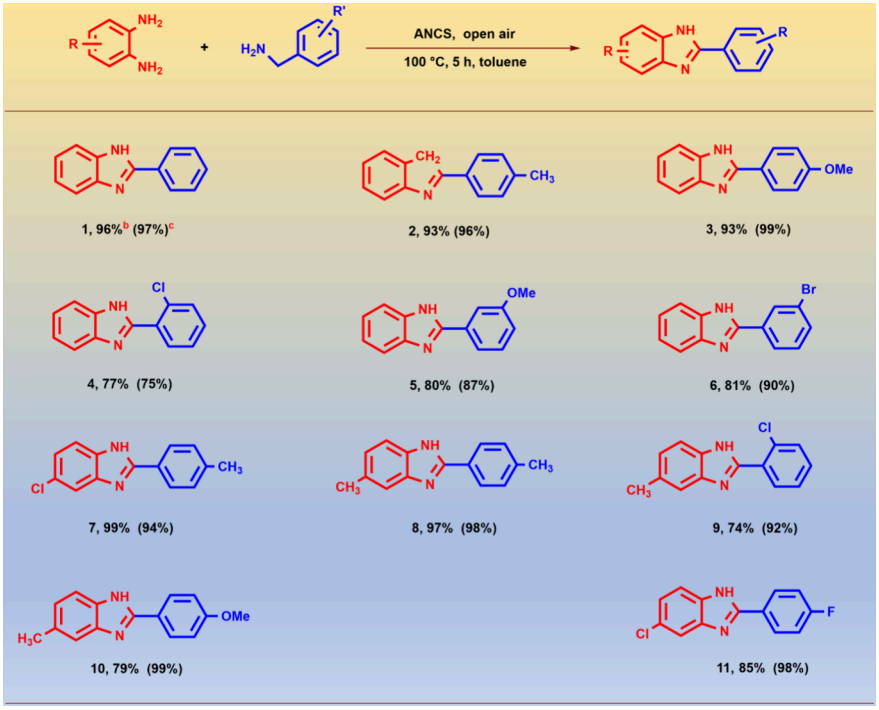

[a]1.5 mmol OPD, 2.5 mmol benzylamine, 15 wt % catalyst with respect to OPD, 100 °C, 5 h, toluene (1 mL), and open-air conditions. [b]OPD conversion. [c]Benzimidazole selectivity.

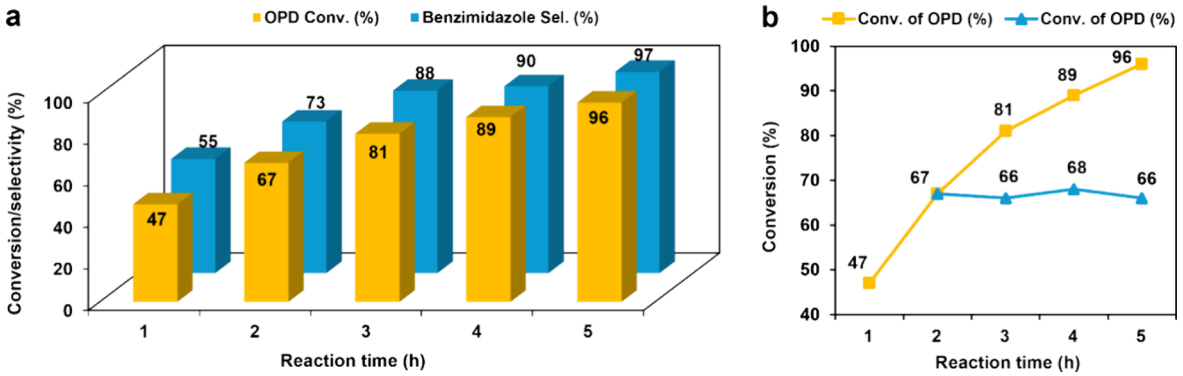

Figure 7. (a) Kinetic studies (reaction conditions: 1.5 mmol of *o*-phenylenediamine (OPD), 2.5 mmol of benzylamine, 15 wt % catalyst with respect to the OPD, 100 °C, 1 mL of toluene, and open-air conditions) and (b) hot-filtration test using the ANCS catalyst (reaction conditions: 1.5 mmol of *o*-phenylenediamine (OPD), 2.5 mmol of benzylamine, 15 wt % catalyst with respect to the OPD, 100 °C, 1 mL of toluene, and open-air conditions).

conversion. The maximum conversion of OPD (96%) with 97% selectivity to benzimidazole was obtained at 5 h. The hot-filtration test was performed to elucidate the stability of the ANCS catalyst in the C−N condensation of the OPD and benzylamine (Figure 7b). Initially, the reaction was conducted for 2 h, and then the ANCS catalyst was removed from the reaction mixture by centrifugation. The reaction was continued for another 3 h using the obtained catalyst-free filtrate at the same reaction conditions. The conversion of OPD remains the same almost after removing the catalyst. Hence, the leaching of the active sites has not occurred, and the reaction is truly heterogeneous, emphasizing the stability of the ANCS catalyst.

4.3. C−N Coupling of Diverse Benzylamines and OPDs Using the ANCS catalyst. The versatile catalytic efficacy of the ANCS material was demonstrated for the C−N coupling of various substituted benzylamines and OPDs (Table 2). The cross-coupling of model compounds, such as benzylamine and OPD, gave 96% conversion with 97% selectivity to benzimidazole (entry 1, Table 2). With this reference, the ANCS catalyst showed reasonably good activity in the C−N condensation of para-substituted benzylamines with OPD (entries 2 and 3, Table 2). In the case of C−N condensation of ortho- and meta-substituted benzylamines with OPD, low conversions/selectivities were obtained irrespective of the substituents' nature (entries 4−6, Table 2). It indicates that the steric hindrance over the electronic effects of the substituents is a dominating factor in the condensation of substituted benzylamines with OPD over the ANCS catalyst. Optimum conversions/selectivities were obtained when both OPD and benzylamine contained the substituents at meta and para positions, respectively (entries 7 and 8, Table 2). In the case of ortho-chloro benzylamine and meta-methyl OPD (entry 9, Table 2), 74% conversion of OPD

https://doi.org/10.1021/acsomega.4c03987
ACS Omega 2024, 9, 35676−35685

Table 3. Benzylamine Homocoupling Using the ANCS Catalyst[a]

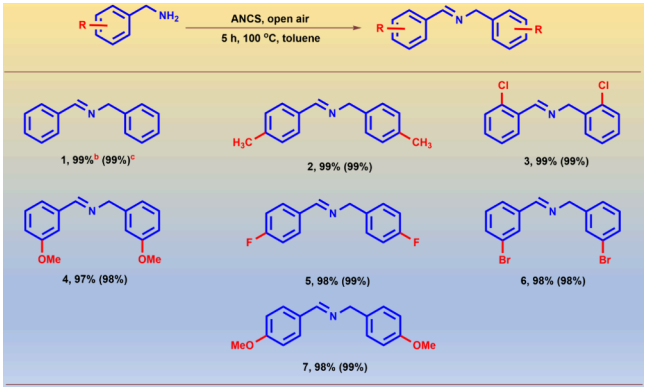

[a]1 mmol benzylamine, 10 wt % catalyst, 100 °C, 5 h, toluene (1 mL), and open-air conditions. [b]Benzylamine conversion. [c]Imine selectivity.

with 92% selectivity to benzimidazole was obtained at 5 h, which is due to the steric hindrance of the substituents. Optimum selectivity to benzimidazole (99%) was obtained when the para-substituted benzylamines reacted with the meta-substituted OPD (entries 10 and 11, Table 2). Overall, the ANCS catalyst showed great potential for the condensation of various benzylamines and OPDs to produce functional benzimidazoles at metal-free and open-air conditions.

4.4. Benzylamine Homocoupling Using the ANCS Catalyst. To further understand the catalytic role of ANCS nanomaterial in the C−N condensation reactions under open-air conditions, we conducted the homocoupling of various benzylamines, which is a pivotal reaction to obtain valuable imines for the pharma industry.[43] The reaction conditions, including temperature, time, and catalyst amount, were optimized to achieve maximum conversion/selectivity in benzylamine homocoupling. The probable reaction mechanism is presented in the Supporting Information (Figure S3).[43] The complete conversion of benzylamine with 99% selectivity to imine was obtained at 100 °C for 5 h in an open-air atmosphere with toluene as the solvent (entry 1, Table 3), whereas only a 2% conversion of benzylamine was noticed in the case of a blank test (i.e., without the catalyst). This emphasizes the catalytic role of the ANCS nanomaterial in benzylamine homocoupling under open-air conditions. Irrespective of the position and nature of the substituents on benzylamine, optimum conversions and/or selectivity were obtained over the ANCS catalyst (entries 2−7, Table 3). Unlike the C−N condensation of benzylamine with an OPD (Table 2), the effect of steric hindrance of the substituents is not observed in the case of benzylamine homocoupling.

The probable mechanism for the C−N coupling of benzylamine with OPD is shown in Figure 8.[43−45] Here, the oxidation of benzylamine using atmospheric air takes place to produce a benzaldehyde intermediate. Then, one of the NH_2 groups of OPD, which acts as a nucleophile, reacts with benzaldehyde to

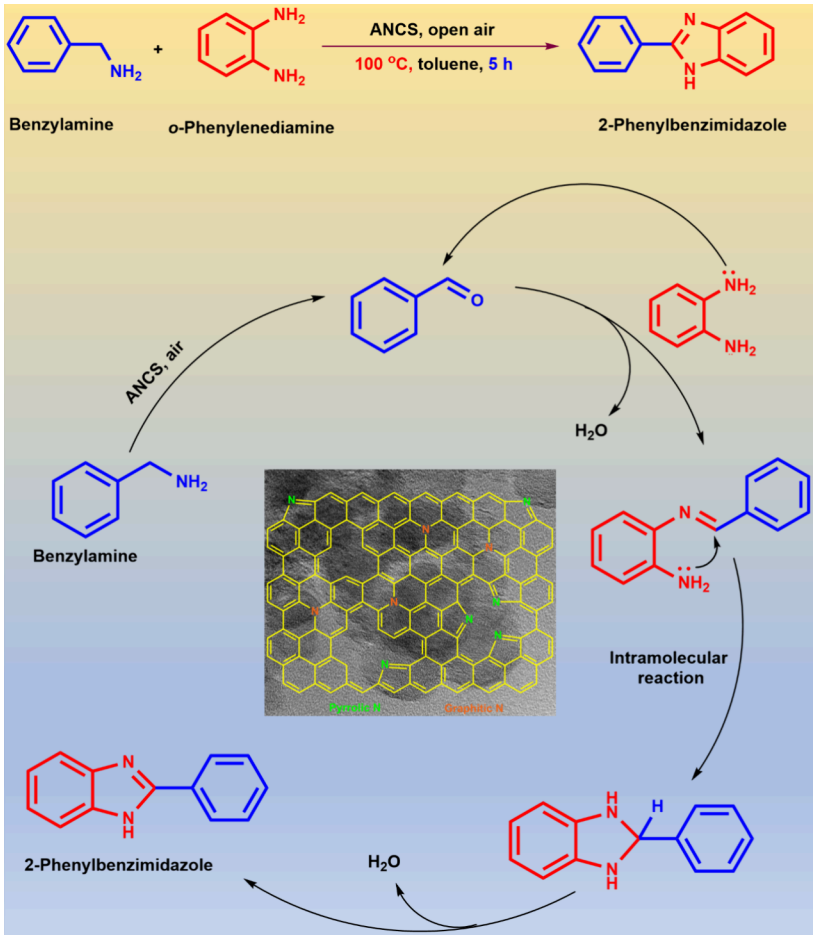

Figure 8. Schematic representation of coupling of benzylamine with an OPD to form benzimidazole over the ANCS catalyst.

https://doi.org/10.1021/acsomega.4c03987
ACS Omega 2024, 9, 35676−35685

give an imine intermediate with water as a byproduct. The subsequent intramolecular C−N condensation, followed by the release of water, gives the desired benzimidazole product. Several controlled reactions between benzylamine and OPD were conducted to estimate the formation of the benzaldehyde intermediate. About 2−3% selectivity of benzaldehyde was noticed, indicating that benzaldehyde reacts with the OPD as soon as it forms from benzylamine.[44,45] However, the identification of benzaldehyde supports the proposed mechanism in Figure 8. In this probable mechanism, the formation of benzaldehyde from benzylamine and the subsequent activation of benzaldehyde to couple with the OPD can be accelerated by the acid and defect sites of the carbon catalyst. Zhao et al. found that the defects and high BET surface area can contribute to the adsorption and activation of oxygen over a carbon catalyst, which is crucial for the oxidative coupling of amines.[43] Raman studies showed that the ANCS catalyst contains a higher number of defect sites due to the synergistic effect of N-doping and KOH activation (Figure 4b). Naturally, the defect sites are electron-deficient, thus they can activate benzylamine and intermediates (benzaldehyde) to facilitate the forward reaction steps in the C−N coupling of benzylamine with OPD. XPS studies provided a piece of evidence for the presence of pyrrolic-N and graphitic-N species in the ANCS catalyst (Figure 5c). Both pyrrolic-N and graphitic-N species are found to provide active sites for the oxidative C−N condensation of amines.[2,26] Moreover, the π electrons of pyrrolic-N atoms can enhance the interaction of the ANCS catalyst with the electron-deficient intermediates (e.g., benzaldehyde and imine), accelerating the reaction toward benzimidazole formation.[27] The pyridine-adsorbed FT-IR studies indicated that the ANCS catalyst contains strong FT-IR peaks belonging to the Lewis acid sites (Figure 6). The C−N coupling reactions are catalyzed by the Lewis acid sites, explaining the excellent activity of the ANCS catalyst. Therefore, it is concluded that the higher concentration of defect sites, functional N-heterocyclic structures, and higher amount of Lewis acid sites are the reasons for the excellent catalytic activity of the ANCS nanomaterial in the selective C−N condensation reactions under metal-free and open-air conditions. The literature comparison revealed (Table S2, Supporting Information) that the ANCS catalyst gave optimum yields of 2-phenylbenzimidazole (94%) at milder reaction conditions without using any external oxidant (entry 4, Table S2, Supporting Information). In contrast, the literature reports used homogeneous, expensive, and metal-based catalysts, higher reaction temperatures (100−130 °C), longer reaction times (5−12 h), and molecular oxygen as the oxidant (entries 1−3, Table S2, Supporting Information). This indicates the significance of the ANCS catalyst, which is active for the C−N coupling reaction under open-air conditions at 100 °C and 5 h (entry 4, Table S2, Supporting Information).

5. CONCLUSIONS

We successfully developed an efficient metal-free carbon catalyst for the selective C−N coupling of amines under open-air conditions. The ANCS catalyst prepared by N-doping and KOH activation showed excellent activity in selective C−N bond formation, which was attributed to more defects, functional N-based groups, and Lewis acid sites. The ANCS catalyst contains well-defined carbon nanospheres, and the nitrogen species are uniformly distributed in the carbon framework. The ANCS catalyst does not show any leaching of the active sites as confirmed by a hot-filtration test, indicating its practical application for the C−N condensation reactions under metal-free and air conditions. The broad application of the ANCS catalyst is showcased for the synthesis of diverse benzimidazoles and imines under mild conditions.

■ ASSOCIATED CONTENT

Supporting Information

The Supporting Information is available free of charge at https://pubs.acs.org/doi/10.1021/acsomega.4c03987.

Experimental section; N_2 adsorption−desorption isotherms; BET surface area, pore volume, and pore diameter; EPR spectra; the probable reaction mechanism for homocoupling of benzylamine; and the comparison of the activity of the ANCS catalyst with that of the literature reports for the C−N coupling of OPD with benzylamine (PDF)

■ AUTHOR INFORMATION

Corresponding Author

Putla Sudarsanam − *Department of Chemistry, Indian Institute of Technology Hyderabad, Kandi, Telangana 502284, India;* orcid.org/0000-0001-5574-2819; Email: sudarsanam.putla@chy.iith.ac.in

Authors

Kumar Krishan − *Department of Chemistry, Indian Institute of Technology Hyderabad, Kandi, Telangana 502284, India*

Bhattu Swapna − *Department of Chemistry, Indian Institute of Technology Hyderabad, Kandi, Telangana 502284, India*

Ankit Kumar Chourasia − *Department of Chemical Engineering, Indian Institute of Technology Hyderabad, Kandi, Telangana 502284, India*

Chandra S. Sharma − *Department of Chemical Engineering, Indian Institute of Technology Hyderabad, Kandi, Telangana 502284, India;* orcid.org/0000-0003-3821-1471

Complete contact information is available at: https://pubs.acs.org/10.1021/acsomega.4c03987

Notes

The authors declare no competing financial interest.

■ ACKNOWLEDGMENTS

B.S. is thankful to the PMRF and MHRD for providing fellowship. P.S. acknowledges the funding support from the SERB-CRG (CRG/2022/005932).

■ REFERENCES

(1) Liu, L.; Corma, A. Metal Catalysts for Heterogeneous Catalysis: From Single Atoms to Nanoclusters and Nanoparticles. *Chem. Rev.* **2018**, *118* (10), 4981−5079.

(2) Rangraz, Y.; Heravi, M. M. Recent Advances in Metal-Free Heteroatom-Doped Carbon Heterogeneous Catalysts. *RSC Adv.* **2021**, *11* (38), 23725−23778.

(3) Wang, W.; Ma, L.; Wang, H.; Jiang, X.; He, Z.-H.; Wang, K.; Yang, Y.; Li, L.; Liu, Z.-T. Tridoped Mesoporous Carbon as a Metal-Free Catalyst for Ammoxidation of (Hetero)Aromatic Alcohols to Nitriles. *ACS Appl. Nano Mater.* **2023**, *6* (16), 15193−15203.

(4) Wu, C.; Bu, J.; Wang, W.; Shen, H.; Cao, Y.; Zhang, H. Imine Synthesis by Benzylamine Self-Coupling Catalyzed by Cerium-Doped MnO_2 under Mild Conditions. *Ind. Eng. Chem. Res.* **2022**, *61* (16), 5442−5452.

(5) Zhang, M.; Wu, S.; Bian, L.; Cao, Q.; Fang, W. One-Pot Synthesis of Pd-Promoted Ce−Ni Mixed Oxides as Efficient Catalysts for Imine

Production from the Direct *N*-Alkylation of Amine with Alcohol. *Catal. Sci. Technol.* **2019**, *9* (2), 286−301.
(6) He, L.; Lou, X.; Ni, J.; Liu, Y.; Cao, Y.; He, H.; Fan, K. Efficient and Clean Gold-Catalyzed One-Pot Selective N-Alkylation of Amines with Alcohols. *Chem. − Eur. J.* **2010**, *16* (47), 13965−13969.
(7) He, L.; Qian, Y.; Ding, R.; Liu, Y.; He, H.; Fan, K.; Cao, Y. Highly Efficient Heterogeneous Gold-catalyzed Direct Synthesis of Tertiary and Secondary Amines from Alcohols and Urea. *ChemSusChem* **2012**, *5* (4), 621−624.
(8) Mavvaji, M.; Akkoc, S. Recent Advances in the Application of Heterogeneous Catalysts for the Synthesis of Benzimidazole Derivatives. *Coord. Chem. Rev.* **2024**, *505*, No. 215714.
(9) Kalbande, P. N.; Singh, N.; Swapna, B.; Umbarkar, S.; Sudarsanam, P. One-Pot Synthesized Efficient Molybdenum-niobium-Oxide Nanocatalyst for Selective C-O and C-N Coupling Reactions at Mild Conditions. *Catal. Commun.* **2023**, *183*, No. 106766.
(10) Marakatti, V. S.; Sarma, S. Ch.; Joseph, B.; Banerjee, D.; Peter, S. C. Synthetically Tuned Atomic Ordering in PdCu Nanoparticles with Enhanced Catalytic Activity toward Solvent-Free Benzylamine Oxidation. *ACS Appl. Mater. Interfaces* **2017**, *9* (4), 3602−3615.
(11) Arun Kumar, M.; Kamali, M.; Putla, S. B.; Subha, P.; Sudarsanam, P. $Nb_2O_5/Ce_{1-x}Nb_xO_{2-\delta}$ Nanorod Catalyst for Selective Oxidative Coupling of Aromatic Alcohols and Amines. *ACS Appl. Nano Mater.* **2024**, *7* (6), 5899−5911.
(12) Singh, N.; Putla, S. B.; Pratap Singh, C.; Kalbande, P. N.; Choudhary, P.; Krishnamurty, S.; Krishnan, V.; Bhatte, K.; Sudarsanam, P. Shape-Controlled MoO_3/MnO_x Nanocatalyst for the Selective Synthesis of 2-Phenylquinoxaline Drug Motifs. *ACS Appl. Nano Mater.* **2023**, *6* (24), 23442−23453.
(13) Ge, C.; Sang, X.; Yao, W.; Zhang, L.; Wang, D. Unsymmetrical Indazolyl-Pyridinyl-Triazole Ligand-Promoted Highly Active Iridium Complexes Supported on Hydrotalcite and Its Catalytic Application in Water. *Green Chem.* **2018**, *20* (8), 1805−1812.
(14) Al-Hmoud, L.; Jones, C. W. Reaction Pathways over Copper and Cerium Oxide Catalysts for Direct Synthesis of Imines from Amines under Aerobic Conditions. *J. Catal.* **2013**, *301*, 116−124.
(15) Huang, S.; Zhao, Z.; Wei, Z.; Wang, M.; Chen, Y.; Wang, X.; Shao, F.; Zhong, X.; Li, X.; Wang, J. Targeted Regulation of the Selectivity of Cascade Synthesis towards Imines/Secondary Amines by Carbon-Coated Co-Based Catalysts. *Green Chem.* **2022**, *24* (18), 6945−6954.
(16) Liu, X.; Dai, L. Carbon-Based Metal-Free Catalysts. *Nat. Rev. Mater.* **2016**, *1* (11), 16064.
(17) Pahra, S.; Sangabathula, O.; Sharma, C. S.; Devi, P. A Noble Metal-Free Candle Soot Derived Carbon Electrocatalyst for Simultaneous H_2 Generation and Wastewater Treatment. *J. Phys. Chem. Solids* **2023**, *173*, No. 111106.
(18) Chourasia, A. K.; Shavez, M.; Naik, K. M.; Bongu, C.; Sharma, C. S. Candle Soot Nanoparticles versus Multiwalled Carbon Nanotubes as a High-Performance Cathode Catalyst for $Li-CO_{2Mars}$ Batteries for Mars Exploration. *ACS Appl. Energy Mater.* **2023**, *6* (1), 378−386.
(19) Zhang, P.; Qiao, Z.-A.; Dai, S. Recent Advances in Carbon Nanospheres: Synthetic Routes and Applications. *Chem. Commun.* **2015**, *51* (45), 9246−9256.
(20) Nieto-Márquez, A.; Romero, R.; Romero, A.; Valverde, J. L. Carbon Nanospheres: Synthesis, Physicochemical Properties and Applications. *J. Mater. Chem.* **2011**, *21* (6), 1664−1672.
(21) Wang, J.; Kaskel, S. KOH Activation of Carbon-Based Materials for Energy Storage. *J. Mater. Chem.* **2012**, *22* (45), 23710.
(22) Li, M.; Xu, F.; Li, H.; Wang, Y. Nitrogen-Doped Porous Carbon Materials: Promising Catalysts or Catalyst Supports for Heterogeneous Hydrogenation and Oxidation. *Catal. Sci. Technol.* **2016**, *6* (11), 3670−3693.
(23) Fiorio, J. L.; Garcia, M. A. S.; Gothe, M. L.; Galvan, D.; Troise, P. C.; Conte-Junior, C. A.; Vidinha, P.; Camargo, P. H. C.; Rossi, L. M. Recent Advances in the Use of Nitrogen-Doped Carbon Materials for the Design of Noble Metal Catalysts. *Coord. Chem. Rev.* **2023**, *481*, No. 215053.
(24) Kaare, K.; Yu, E.; Volperts, A.; Dobele, G.; Zhurinsh, A.; Dyck, A.; Niaura, G.; Tamasauskaite-Tamasiunaite, L.; Norkus, E.; Andrulevičius, M.; Danilson, M.; Kruusenberg, I. Highly Active Wood-Derived Nitrogen-Doped Carbon Catalyst for the Oxygen Reduction Reaction. *ACS Omega* **2020**, *5* (37), 23578−23587.
(25) Shi, Z.; Yang, W.; Gu, Y.; Liao, T.; Sun, Z. Metal-Nitrogen-Doped Carbon Materials as Highly Efficient Catalysts: Progress and Rational Design. *Adv. Sci.* **2020**, *7* (15), No. 2001069.
(26) Wang, K.; Jiang, P.; Yang, M.; Ma, P.; Qin, J.; Huang, X.; Ma, L.; Li, R. Metal-Free Nitrogen-Doped Carbon Nanosheets: A Catalyst for the Direct Synthesis of Imines under Mild Conditions. *Green Chem.* **2019**, *21* (9), 2448−2461.
(27) Bang, G. S.; Shim, G. W.; Shin, G. H.; Jung, D. Y.; Park, H.; Hong, W. G.; Choi, J.; Lee, J.; Choi, S.-Y. Pyridinic-N-Doped Graphene Paper from Perforated Graphene Oxide for Efficient Oxygen Reduction. *ACS Omega* **2018**, *3* (5), 5522−5530.
(28) Kakunuri, M.; Sharma, C. S. Candle Soot Derived Fractal-like Carbon Nanoparticles Network as High-Rate Lithium Ion Battery Anode Material. *Electrochim. Acta* **2015**, *180*, 353−359.
(29) Tsai, C.-Y.; Tai, H.-C.; Su, C.-A.; Chiang, L.-M.; Li, Y.-Y. Activated Microporous Carbon Nanospheres for Use in Supercapacitors. *ACS Appl. Nano Mater.* **2020**, *3* (10), 10380−10388.
(30) Luo, H.; Lv, Y.; Tian, S.; Li, G.; Dai, W. Metal-Free Nitrogen-Doped Porous Carbons for Nitriles and Amides Synthesis from 1,2-Diols via Oxidative Cleavage of C−C Bonds. *ACS Catal.* **2023**, *13* (22), 14996−15006.
(31) Zhou, Q.; Guo, X.; Song, C.; Zhao, Z. Defect-Enriched N,O-Codoped Nanodiamond/Carbon Nanotube Catalysts for Styrene Production via Dehydrogenation of Ethylbenzene. *ACS Appl. Nano Mater.* **2019**, *2* (4), 2152−2159.
(32) Li, X.; Luo, W.; Zhu, K.; Chen, Y.; Huang, Y.; Jin, C.; Qiu, R.; Luo, S.; Guan, G.; Yan, K. Electronic Modulation of S and N Co-Implanted Carbon as Fenton-like Photocatalysts for Water Remediation. *Chem. Eng. J.* **2023**, *474*, No. 146016.
(33) Várhegyi, G.; Szabó, P.; Till, F.; Zelei, B.; Antal, M. J.; Dai, X. TG, TG-MS, and FTIR Characterization of High-Yield Biomass Charcoals. *Energy Fuels* **1998**, *12* (5), 969−974.
(34) Schuepfer, D. B.; Badaczewski, F.; Guerra-Castro, J. M.; Hofmann, D. M.; Heiliger, C.; Smarsly, B.; Klar, P. J. Assessing the Structural Properties of Graphitic and Non-Graphitic Carbons by Raman Spectroscopy. *Carbon* **2020**, *161*, 359−372.
(35) Ottaviani, M. F.; Mazzeo, R. EPR Characterization of Graphitized and Activated Micro- and Meso-porous Carbons. *Microporous Mesoporous Mater.* **2011**, *141*, 61−68.
(36) Yang, M.; Guo, D.; Zhang, T.; Liu, G.; Wu, N.; Qin, A.; Liu, X.; Mi, H. Controlled Synthesis of Ultrafine β-Mo_2C Nanoparticles Encapsulated in N-Doped Porous Carbon for Boosting Lithium Storage Kinetics. *ACS Omega* **2021**, *6* (44), 29609−29617.
(37) Vashchynskyi, V.; Okhay, O.; Boychuk, T. Chemical Activation of Apricot Pit-Derived Carbon Sorbents for the Effective Removal of Dyes in Environmental Remediation. *C (Basel)* **2023**, *9* (4), 93.
(38) Hu, M.; Ye, Z.; Zhang, Q.; Xue, Q.; Li, Z.; Wang, J.; Pan, Z. Towards Understanding the Chemical Reactions between KOH and Oxygen-Containing Groups during KOH-Catalyzed Pyrolysis of Biomass. *Energy* **2022**, *245*, No. 123286.
(39) El-Hendawy, A.-N. A. Variation in the FTIR Spectra of a Biomass under Impregnation, Carbonization and Oxidation Conditions. *J. Anal Appl. Pyrolysis* **2006**, *75* (2), 159−166.
(40) Salinas-Torres, D.; Navlani-García, M.; Mori, K.; Kuwahara, Y.; Yamashita, H. Nitrogen-Doped Carbon Materials as a Promising Platform toward the Efficient Catalysis for Hydrogen Generation. *Appl. Catal. A Gen.* **2019**, *571*, 25−41.
(41) Zheng, Y.; Wang, J.; Li, D.; Liu, C.; Lu, Y.; Lin, X.; Zheng, Z. Insight into the $KOH/KMnO_4$ Activation Mechanism of Oxygen-Enriched Hierarchical Porous Biochar Derived from Biomass Waste by in-Situ Pyrolysis for Methylene Blue Enhanced Adsorption. *J. Anal Appl. Pyrolysis* **2021**, *158*, No. 105269.
(42) Ji, N.; Yin, J.; Rong, Y.; Li, H.; Yu, Z.; Lei, Y.; Wang, S.; Diao, X. More than a Support: The Unique Role of Nb_2O_5 in Supported Metal

https://doi.org/10.1021/acsomega.4c03987
ACS Omega 2024, 9, 35676−35685

Catalysts for Lignin Hydrodeoxygenation. *Catal. Sci. Technol.* **2022**, *12* (12), 3751−3766.
(43) Zhao, J.-X.; Wang, W.; Jiao, Z.-F.; Guo, X.-Y. A Highly Efficient Defective Carbon Catalyst for Oxidative Coupling of Amines. *Catal. Commun.* **2023**, *177*, No. 106652.
(44) Li, F.; Dai, X.; Qi, W. Primary Amine Coupling on Nanocarbon Catalysts: Reaction Mechanism and Kinetics via Fluorescence Probe Analysis. *Green Energy Environ.* **2020**, *5* (4), 453−460.
(45) Tashrifi, Z.; Khanaposhtani, M. M.; Larijani, B.; Mahdavi, M. Recent Advances in the Oxidative Conversion of Benzylamines. *Tetrahedron* **2021**, *84*, No. 131990.

https://doi.org/10.1021/acsomega.4c03987
ACS Omega 2024, 9, 35676−35685